Supplementary Information (SI) for Energy Advances.

Supplementary Information - Decoding the $AlPO_4$ and LATP surface with a combined NMR-DFT approach

Javier Valenzuela Reina[ad*], Vera M. Barysch[bc*], Conrad Szczuka[b], Simone S. Köcher[ba‡], Josef Granwehr[bc] and Christoph Scheurer[ab]

1 Further details on materials and methods

1.1 Sample preparation

1.1.1 $AlPO_4$

To provide more data points, additional $AlPO_4$ (99.99 % trace metal basis, Sigma-Aldrich) samples have been dried for 0.5 h, 1.5 h, and 17 h using the same procedure. The corresponding spectra can be found in Section 2.2.

The CPMAS and the TRAPDOR experiments were conducted with the $AlPO_4$ powder that was dried for 63 h at 120 °C. Prior to conducting the CP experiments, it was stored under argon atmosphere.

1.1.2 Silanization of $AlPO_4$ and LATP

$AlPO_4$ (99.99 % trace metal basis, Sigma-Aldrich, dried for 17 h) was dispersed in toluene. For 100 mg of the inorganic powder, roughly 10 mL of toluene was added as a dispersant. Detailed information about the quantities of the reactants are given in Tab. S1. Trimethoxy-(2-phenylethyl)silane (TMPES, Sigma-Aldrich) was added and the mixture was stirred at 120 °C for 4 h. The product was centrifuged and washed with toluene (2x2 mL), cyclohexane (6x2 mL) and ethanol (4x2 mL). It was dried at 60 °C and 100 mbar overnight.

Also, lithium aluminium titanium phosphate $Li_{1+x}Al_xTi_{2-x}(PO_4)_3$ (LATP) with $x = 0.5$ was silanized. The LATP was synthesized from $LiOH \cdot H_2O$, $Ti[OCH(CH_3)_2]_4$, H_3PO_4 and $Al[OOCH_3(OH)_2] \cdot xH_2O$. Afterwards, it was calcined at 500 °C, sintered at 900 °C, and stored under argon atmosphere. Davaasuren *et al.* provided detailed information about the synthesis route.[72] The mixing and stirring for the silanization of LATP was conducted under argon atmosphere, the temperature was reduced to 70 °C and the reaction time was prolonged to overnight. The weight of the reactants and products (Tab. S1) reveals that the loss of ceramic material during the workup is larger than the weight gain due to silanization.

Table S1 Weights of reactants before silanization and weights of silanized samples

Substrate	Silane	$m_{\text{substrate}}$ / mg	m_{silane} / mg	n_{silane} / mmol	m_{product} / mg
$AlPO_4$	TMPES	90	226	1.0	70
LATP	TMPES	99	226	1.0	68

The samples were packed into MAS rotors (3.2 mm in diameter) under argon atmosphere.

1.2 NMR measurements

The NMR experiments were conducted on a Bruker Avance III HD spectrometer with a 9.4 T magnet and processed using Bruker TopSpin v3.6.2. The processing involved baseline corrections, phase corrections, and apodization.

1.2.1 ^{1}H, ^{31}P, and ^{27}Al MAS NMR

The measurement parameters were chosen as listed in Tab. S2, which also provides the parameters for the measurement of pure TMPES. All ^{1}H MAS NMR spectra were acquired by applying a Hahn Echo sequence with the excitation pulse length $p_1 = 4.6$ μs, the refocussing pulse length $p_2 = 9.2$ μs, and a power level of PLW1 = 19.011 W. The samples were measured at a spinning frequency of 20 kHz if not stated differently. ^{1}H MAS NMR spectra were referenced to TMS at 0 ppm and ^{31}P MAS NMR spectra to $NH_4H_2PO_4$ at 1.0 ppm[73] (spectra shown in Fig. 5 and S7) or to 85 % H_3PO_4 at 0 ppm (Fig. 6).[74] ^{27}Al MAS NMR spectra were referenced to the hexaaquaaluminium ion at 0 ppm[75]. In order to normalize and compare the later spectra, the rotor contents were weighed.

---

[a] *Fritz-Haber Institute of the Max Planck Society, 14195 Berlin, Germany*
[b] *Institute of Energy Technologies (IET-1), Forschungszentrum Jülich GmbH, Jülich, Germany*
[c] *Institute of Technical and Macromolecular Chemistry, RWTH Aachen University, 52056 Aachen, Germany*

[*] These authors contributed equally to this work.

[‡] Corresponding author

Table S2 NMR acquisition parameters of the measurements: pulse length p_1, power level PLW1, delay time d_1, dwell time DW, number of dummy scans DS and number of scans NS

Sample	Nucleus	p_1 / μs	PLW1 / W	d_1 / s	DW / μs	DS	NS
$AlPO_4$	^1H	4.60	19.011	5.0	2.500	0	32
	^{27}Al	1.70	100.000	2.0	6.133	4	128
	^{31}P	3.65	38.905	10.0	6.133	4	64
Silanized LATP	^1H	4.60	19.011	5.0	2.500	4	256
TMPES	^1H	4.60	19.011	5.0	62.400	4	16

Table S3 Further experimental parameters for the $^{31}P\{^1H\}$ CP measurements of dried $AlPO_4$. As a decoupling sequence the swftppm_13 from Bruker was used with a pulse length of PCPD2 = 4 μs, a decoupling power level of PLW12 = 70 W and a special decoupling power level of 55.744 W. For variable amplitude CP ramp50100.100 was used

Parameter	Value
DW / μs	6.133
90° proton pulse length p_3 / μs	2
d_1 / s	20
NS	64
PLW1 / W	38.905
DS	0

$^{31}P\{^1H\}$ CPMAS NMR experiments were conducted using the $AlPO_4$ sample that was dried for 63 h and then stored under argon atmosphere. Two different contact times (1000 μs and 7000 μs) were measured to study the spatial proximity of ^{31}P nuclei and ^1H nuclei.

1.2.2 TRAPDOR experiments

$^{27}Al\{^1H\}$ TRAPDOR experiments were conducted by measuring ^1H MAS NMR spectra (MAS rate = 5 kHz) both with and without ^{27}Al irradiation for different ^{27}Al frequency offsets O2 in the range of -2.5 MHz up to +2.5 MHz in steps of 0.25 MHz. Also O2=±0.05 MHz and O2=±0.1 MHz were measured. Further details can be found in Tab. S4.

Table S4 Further experimental parameters for the $^{27}Al\{^1H\}$ TRAPDOR experiments of $AlPO_4$

Parameter	Value
MAS spinning frequency / kHz	5
DW / μs	4
p_1 / μs	5
p_2 / μs	10
d_1 / s	5
NS	4
PLW1 / W	16.106
DS	0
F2 mixing pulse p_{15} / μs	192.5
F2 power level PLW2 / W	7.3961

1.3 Computational methods

MagresView v.1.6.2[76] was employed for processing and analyzing the computed NMR properties. The structural models were visualized with VESTA 3.90[77]. The rendered atomic structures were created with the Atomic Simulation Environment[78] python set of modules and PyMol[79].

1.3.1 Calculations

The size of the plane wave basis set in CASTEP[54] v.23 was determined by carrying out convergence tests with a cut-off energy step of 100 eV. An energy cutoff of 1000 eV achieved a converged value for the computed Al and P electric field gradient (EFG) tensor components and isotropic chemical shieldings, with a variation of less than 1% of their computed values with respect to the next computed energy cutoff. The k-point Monkhorst-Pack (MP) grid was built with a density of 0.3 k-points $Å^{-1}$. The atomic coordinates of all the structures were optimized prior to the NMR parameter calculation with an energy and force variation tolerance of 10^{-5} eV/atom and 0.03 eV $Å^{-1}$, respectively.

1.3.2 Bulk simulations

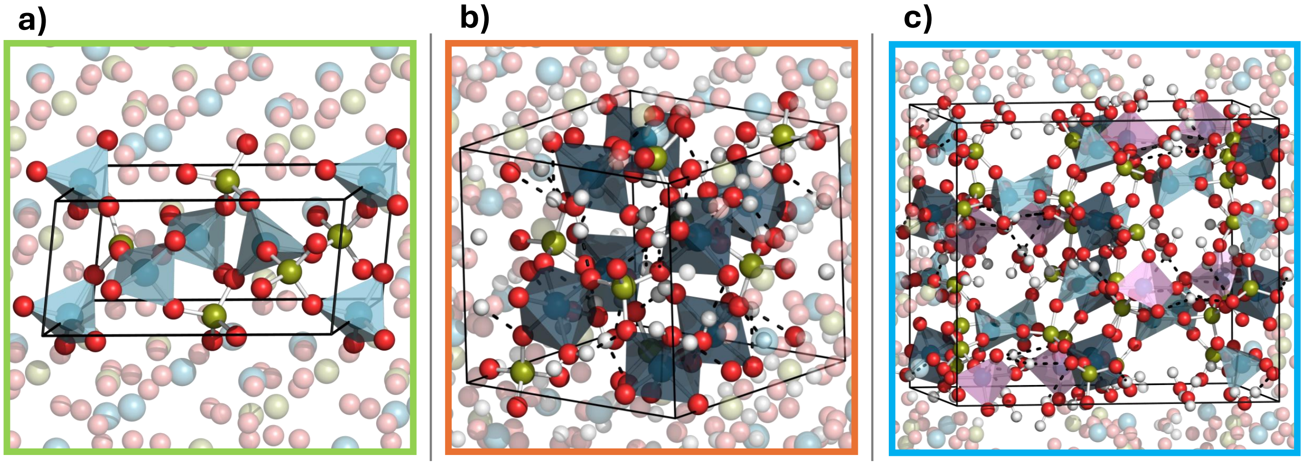

Fig. S1 Unit cells of berlinite ($AlPO_4$) (a), variscite ($AlPO_4 \cdot 2H_2O$) (b), and UiO-7 ($Al_{32}P_{32}O_{128} \cdot 62H_2O$) (c). Al, P, O, and H atoms are represented in blue, green, red, and white, respectively. The 4-fold, 5-fold, and 6-fold coordinated aluminum polyhedra are depicted in light blue, purple, and dark blue, respectively. Hydrogen bonds are depicted by dashed black lines.

1.3.3 Surface simulations

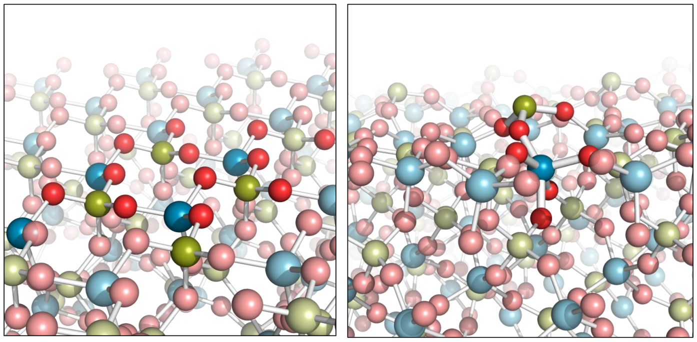

Fig. S2 Structural models of quartz-berlinite(a) and buckled-berlinite(b).

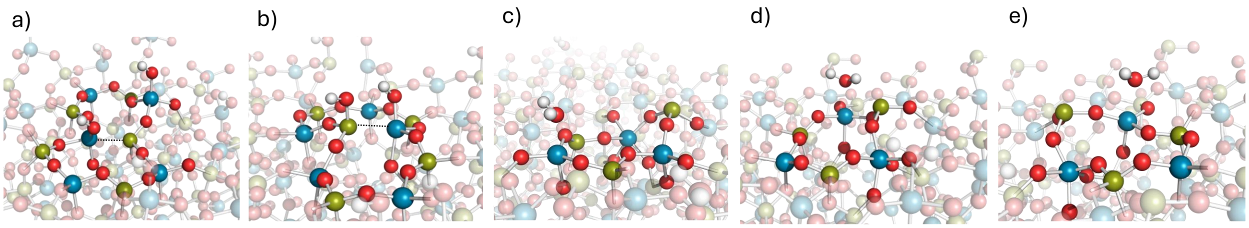

Fig. S3 Structural models of ((Al-OH)(P-OH)-berlinite) (a), (Al-OH)$_2$-berlinite (b), Al$_{\text{middle}}$(H_2O)-berlinite (c), Al$_{\text{low}}$(H_2O)-berlinite (d), and Al$_{\text{high}}$(H_2O)-berlinite (e).

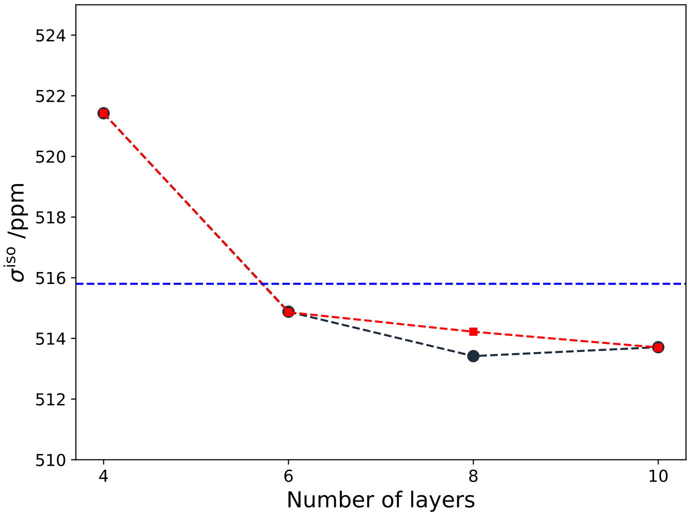

Fig. S4 Convergence of Al σ^{iso} for the first (black) and middle layer (red) of a $AlPO_4$ 001 slab with respect to the slab thickness. The blue dashed horizontal line indicates the calculated ^{27}Al σ^{iso} in the bulk structure.

The slab thickness is converged with respect to the NMR parameters on the surface. The convergence tests (Fig. S4) show that at least six $AlPO_4$ layers are necessary to achieve an inner region in the slab that presents the same NMR parameters as the bulk unit cell structure with a ± 2 ppm margin, along with converged values of the NMR parameters in the surface. For this reason, this thickness is used in the surface study.

Since the use of asymmetric slabs can lead to structures that present a dipolar charge distribution across the vacuum axis, a self-consistent dipole correction scheme[59] is applied that avoids this effect on the calculation of the system energy and electron density. The correction shows a minor impact on the energy values, but has a considerable impact on the isotropic chemical shielding calculation, as observable for σ^{iso} in the first layer of Al atoms, which decreases by 23 % if the correction is not implemented.

2 Further details on results

2.1 Benchmarking DFT study of $AlPO_4$ polymorphs

The comparison of experimental and simulated ^{27}Al quadrupolar coupling constants and chemical shifts for some the known phases of hydrous and anhydrous $AlPO_4$ (berlinite, trydimite, critobalite and variscite) is shown in Tab. S5. The calculated chemical shifts show a reasonable qualitative agreement that allows to establish a relative chemical shift scale of the different Al environments. This study, however, is limited by the scarce number of structural and NMR experimental information available for the polymorphs, which are usually not purely crystalline. A more detailed study needs to also consider the temperature dependence of the observed NMR parameters. The RMSE of the calculated quadrupolar coupling parameters is 0.34 MHz for C_Q and 0.12 for η, where the most significant outlier is the cristobalite polymorph.

Table S5 Overview of ^{27}Al C_Q η, and δ for different $AlPO_4$ phases. The experimental results based on [31,33] are listed as well as the simulated values. The calculate berlinite chemical shift is aligned with the maximum of the observed Al signal in the dried $AlPO_4$ sample at 36 ppm.

	Experimental			Simulated		
	$C_Q(^{27}Al)$ / MHz	$\eta(^{27}Al)$	δ (^{27}Al) / ppm	$C_Q(^{27}Al)$ / MHz	$\eta(^{27}Al)$	δ (^{27}Al) / ppm
berlinite	4.09	0.37	44.5	3.96	0.39	36.00
trydimite	0.75	0.95	39.8	0.74	0.75	36.61
cristobalite	1.2	0.75	42.5	2.35	0.46	41.63
variscite	3.1	0.73	-7.75	3.34	0.47	-11.18

2.2 MAS NMR experiments on $AlPO_4$

The $AlPO_4$ powder samples were measured at different stages of drying. For reasons of clarity, only the limiting cases were discussed in the main paper. Here, the ^{27}Al MAS NMR spectra (Fig. S5a) are depicted with an exemplary integral fitting procedure for the commercial sample (Fig. S5b) and the integral change with the drying time (Fig. S5c). The same figures were created for ^{1}H MAS NMR spectra (Figs. S6a, S6b, and S6c). Moreover, the ^{31}P MAS NMR spectra are shown for all the investigated drying times (Fig. S7).

The ^{27}Al and ^{1}H signals were fitted according to

$$y = y_0 + A\left[\mu \cdot \frac{2}{\pi} \cdot \frac{w}{4(x-\delta)^2 + w^2} + (1-\mu) \cdot \frac{\sqrt{4\ln 2}}{\sqrt{\pi} w} \cdot \exp\left(-\frac{4\ln 2}{w^2}(x-\delta)^2\right)\right] \tag{3}$$

using OriginPro 2021b (OriginLab Corporation, Northampton, MA, USA) with the baseline offset y_0 (here always close to zero), the area A, the Lorentzian fraction μ, the chemical shift (center position) δ, and the full width at half maximum (FWHM) w. The fitting procedure was conducted with constraints on δ and w to reach convergence. The results are summarized in Tabs. S6 and S7.

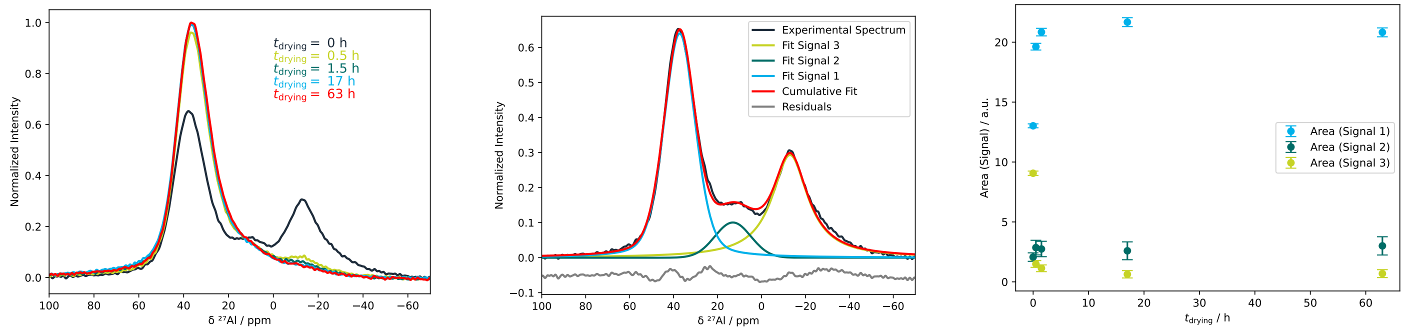

(a) (b) (c)

Fig. S5 ^{27}Al MAS NMR spectra of AlPO$_4$ at different stages of drying for different drying times t_{drying}. In (a), the intensities are normalized to the respective total integral and the maximum intensity of the sample dried for 63 h. The pseudo-Voigt fitting procedure is shown in (b) exemplarily for the ^{27}Al MAS NMR measurement of the commercial sample. (c) The fitted areas of the three signals in the ^{27}Al MAS NMR spectra are plotted against the drying time. The standard errors obtained from the pseudo-Voigt fitting procedure are included as error bars.

Table S6 Fitting parameters of ^{27}Al MAS NMR measurements of AlPO$_4$ at different drying stages

drying time	0 h	0.5 h	1.5 h	17 h	63 h
δ (peak 1) / ppm	37.2 ± 0.1	36.0 ± 0.1	36.0 ± 0.1	36.1 ± 0.1	36.0 ± 0.1
A (peak 1) / a.u.	13.0 ± 0.2	19.6 ± 0.3	20.8 ± 0.4	21.7 ± 0.4	20.8 ± 0.4
w (peak 1) / ppm	16.8 ± 0.1	16.6 ± 0.1	16.7 ± 0.1	16.9 ± 0.1	16.8 ± 0.1
μ (peak 1)	0.37 ± 0.02	0.44 ± 0.02	0.49 ± 0.02	0.0 ± 0.6	0.46 ± 0.02
δ (peak 2) / ppm	13.0 ± 0.2	13.0 ± 0.3	15.0 ± 0.3	14.0 ± 0.4	14.0 ± 0.3
A (peak 2) / a.u.	2.1 ± 0.4	2.9 ± 0.7	2.7 ± 0.7	2.6 ± 0.8	3.0 ± 0.8
w (peak 2) / ppm	19 ± 1	21 ± 2	21 ± 2	23 ± 3	21 ± 2
μ (peak 2)	0.0 ± 0.4	0.0 ± 0.5	0.0 ± 0.5	0.0 ± 0.6	0.0 ± 0.5
δ (peak 3) / ppm	-13.0 ± 0.1	-12.8 ± 0.8	-11.0 ± 1.1	-12.4 ± 1.4	-12.0 ± 2.0
A (peak 3) / a.u.	9.1 ± 0.2	1.5 ± 0.3	1.1 ± 0.3	0.6 ± 0.4	0.7 ± 0.4
w (peak 3) / ppm	20 ± 1	22 ± 2	22 ± 2	19 ± 3	20 ± 4
μ (peak 3)	1.00 ± 0.02	0.0 ± 0.3	0.0 ± 0.4	0.0 ± 0.7	0.0 ± 0.7

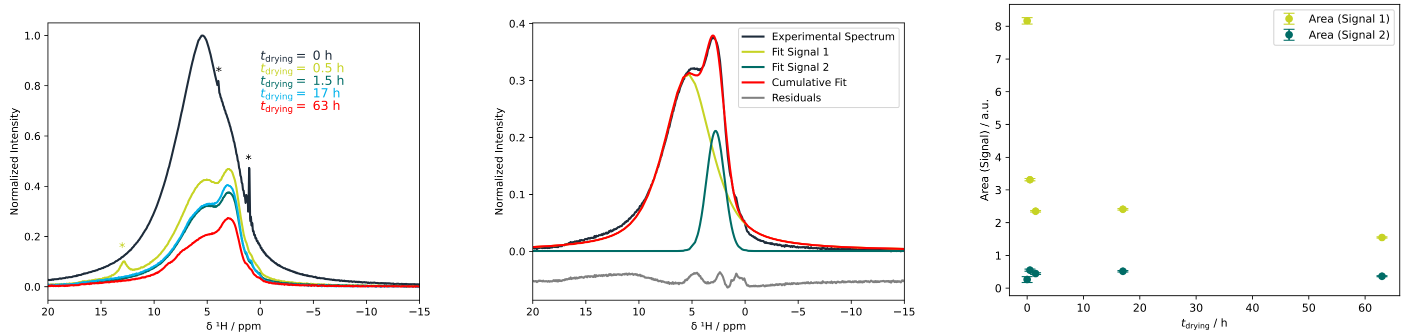

(a) (b) (c)

Fig. S6 ^{1}H MAS NMR spectra of AlPO$_4$ at different stages of drying. In (a), the intensities are normalized to the respective rotor content mass and impurities are denoted by asterisks. The pseudo-Voigt fitting procedure is shown in (b) exemplarily for the ^{1}H MAS NMR measurement of the sample dried for 1.5 h. (c) The fitted areas of the two signals in the ^{1}H MAS NMR spectra are plotted against the drying time. The standard errors obtained from the pseudo-Voigt fitting procedure are included as error bars.

Table S7 Fitting parameters of ^{1}H MAS NMR measurements of $AlPO_4$ at different drying stages

drying time	0 h	0.5 h	1.5 h	17 h	63 h
δ (peak 1) / ppm	5.5 ± 0.1	5.5 ± 0.1	5.4 ± 0.1	5.5 ± 0.1	5.5 ± 0.1
A (peak 1) / a.u.	8.17 ± 0.10	3.31 ± 0.04	2.35 ± 0.03	2.41 ± 0.03	1.55 ± 0.02
w (peak 1) / ppm	5.5 ± 0.1	5.3 ± 0.1	5.4 ± 0.1	5.3 ± 0.1	5.5 ± 0.1
μ (peak 1)	0.89 ± 0.02	0.91 ± 0.02	0.75 ± 0.02	0.81 ± 0.02	0.73 ± 0.02
δ (peak 2) / ppm	2.7 ± 0.1	2.8 ± 0.1	2.8 ± 0.1	2.8 ± 0.1	2.8 ± 0.1
A (peak 2) / a.u.	0.26 ± 0.09	0.55 ± 0.04	0.45 ± 0.03	0.52 ± 0.03	0.36 ± 0.02
w (peak 2) / ppm	2.1 ± 0.2	2.1 ± 0.1	2.0 ± 0.1	2.1 ± 0.1	2.1 ± 0.1
μ (peak 2)	0.0 ± 0.6	0.00 ± 0.09	0.00 ± 0.08	0.00 ± 0.07	0.00 ± 0.07

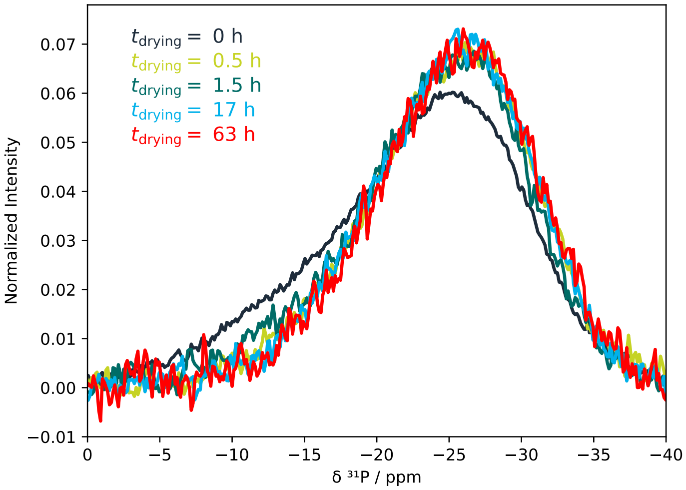

Fig. S7 ^{31}P MAS NMR spectra of $AlPO_4$ at different stages of drying. The intensities are normalized to the respective total integral.

Even though, the experimental samples of $AlPO_4$, both commercial and dried, do not show any predominant crystalline order, but are rather amorphous, the observed shifts of ^{27}Al and ^{31}P are consistent with MAS-NMR results of different $AlPO_4$ phases reported in literature (Tab. S8).

System	Literature	Nucleus	Shift / ppm	FWHM / ppm	Reference	MAS / kHz
quartz-$AlPO_4$	Ladwig *et al.*[33]	^{27}Al	22.6	32	$[Al(H_2O)_6]^{3+}$	3
quartz-$AlPO_4$	Ladwig *et al.*[33]	^{31}P	-25.6	–	H_3PO_4	3
$AlPO_4$-15	Byrne *et al.*[80]	^{27}Al	2.5, -5.0	5	$Al(NO_3)_3$	10
$AlPO_4$-15	Byrne *et al.*[80]	^{31}P	-14.3, -20.5	3	H_3PO_4	13
$AlPO_4$-14A	Brouwer *et al.*[81]	^{27}Al	52.0, 32.5, -19.0	15, 15.5, 9.5	$Al(NO_3)_3$	15
$AlPO_4$-14A	Brouwer *et al.*[81]	^{31}P	-19.0, -28.5	2.0, 2.2	H_3PO_4	15
$AlPO_4$	this work	^{27}Al	36, 14, 12	17, 20, 20	$[Al(H_2O)_6]^{3+}$	20
$AlPO_4$	this work	^{31}P	-25 to -26	13	85 % H_3PO_4	20

Table S8 Literature review of ^{27}Al and ^{31}P MAS NMR spectra of various $AlPO_4$ species. The FWHM of spectral peaks in literature are estimated from the figures.

2.3 MAS NMR experiments on LATP

For basic investigations, MAS NMR experiments on the LATP powder were conducted. These are in good agreement with results in literature. In addition to LATP, these measurements also indicate the presence of $AlPO_4$ as a side phase and possibly further impurities.

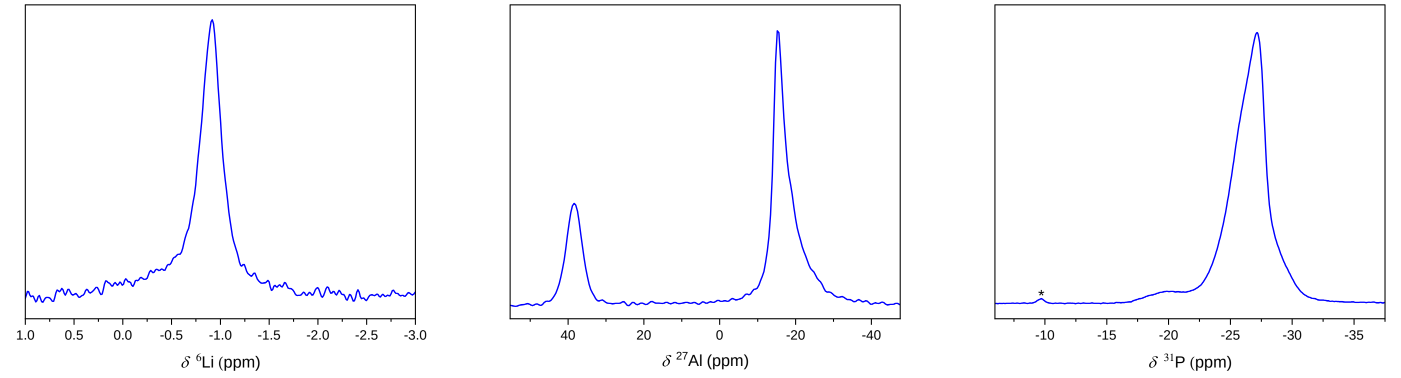

(a) (b) (c)

Fig. S8 a) ^{6}Li MAS NMR, b) ^{27}Al MAS NMR spectrum, and c) ^{31}P MAS NMR spectrum of LATP. All measurements were conducted with a MAS spinning frequency of 20 kHz.

The ^{6}Li MAS NMR spectrum shows one main signal around -1 ppm, which is in agreement with literature for LATP with x=0.5.[82] The ^{27}Al MAS NMR spectrum exhibits two signals with maximum intensities at 39 ppm and -18 ppm, the former resulting from an $AlPO_4$ side phase, and the latter from octahedrally coordinated Al in LATP. Also the ^{31}P MAS NMR spectrum shows a signal centered at 24 ppm similar to the findings of Chandran *et al.*[82], with an additional attribution around -20 ppm due to $AlPO_4$ and an unresolved impurity at -10 ppm, which also occurs in the work by Chandran *et al.*

2.4 SEM and EDX experiments

SEM/EDX measurements provide further prove of successful silanization and are shown in Fig. S9 for $AlPO_4$ and in Fig. S10 for LATP.

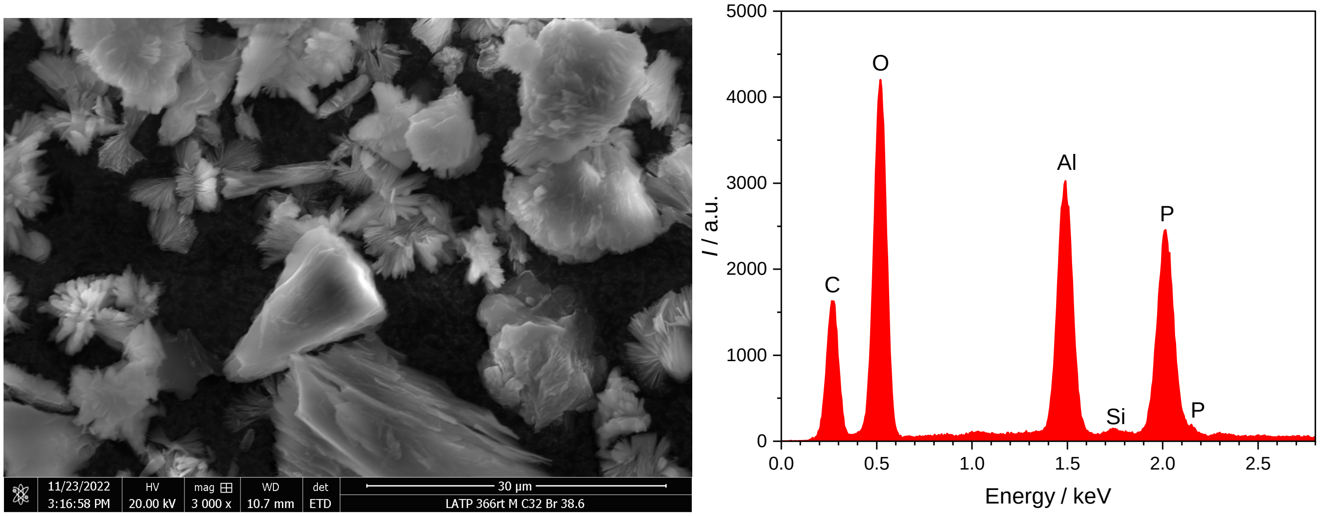

(a) (b)

Fig. S9 (a) SEM image of $AlPO_4$ silanized with TMPES. (b) EDX spectrum of area depicted in (a).

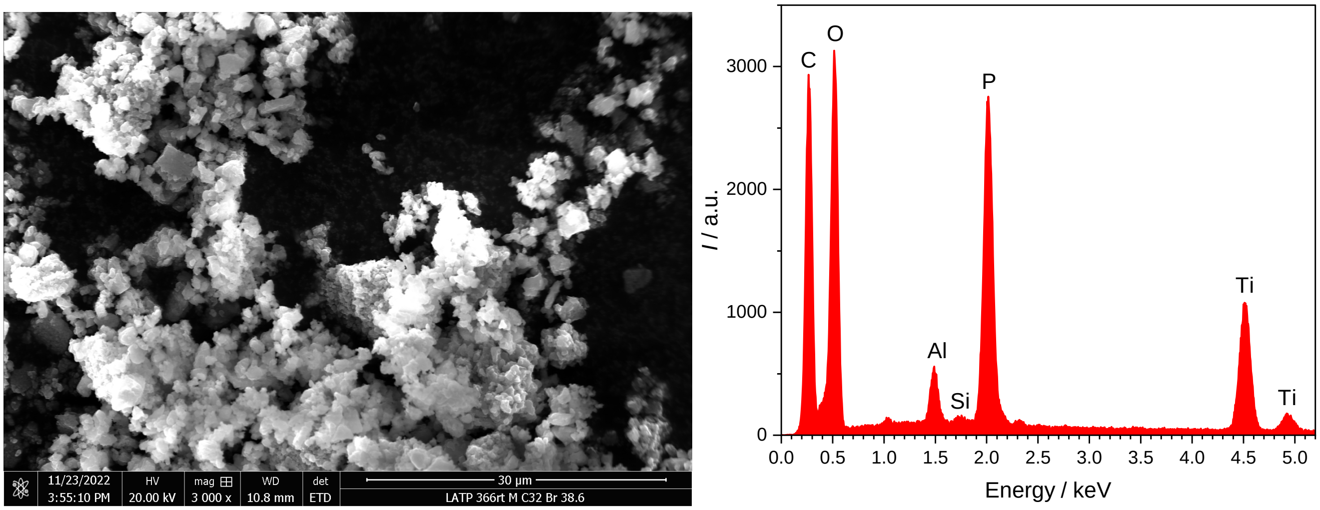

(a) (b)

Fig. S10 (a) SEM image of LATP silanized with TMPES. (b) EDX spectrum of area depicted in (a).

2.5 DFT simulations

Table S9 Summary of NMR DFT simulations of the studied hydrous and anhydrous $AlPO_4$ bulk models. The calculated berlinite chemical shifts are aligned with the maxima of the signals of the ^{27}Al and ^{31}P in the NMR spectrum of the dried $AlPO_4$ sample at 36.00 and -26.30 ppm, respectively.

Structure	Atom	Structural motif	δ ^{27}Al / ppm	C_Q / MHz	η
berlinite	Al	AlO_4	36.00	3.96	0.39
	P	PO_4	-26.30		
UiO-7	Al1	AlO_4	37.19	5.49	0.74
	Al2	$AlO_4 \cdot H_2O$	14.64	8.41	0.59
	Al3	$AlO_4 \cdot 2(H_2O)$	-9.66	6.11	0.34
	P	PO_4	-36.86		
variscite	Al	$AlO_4 \cdot 2(H_2O)$	-11.18	3.34	0.47
	P	PO_4	-25.23		

Table S10 Berlinite slab models with corresponding energies, δ (^{27}Al), C_Q(^{27}Al), and η(^{27}Al) as well as σ^{iso}(^{31}P).The calculated berlinite chemical shifts are aligned with the maxima of the signals of the ^{27}Al and ^{31}P in the NMR spectrum of the dried $AlPO_4$ sample at 36.00 and -26.30 ppm, respectively.

Slab Model	Energy / eV/atom	δ (^{27}Al) / ppm	C_Q(^{27}Al) / MHz	η(^{27}Al)	δ (^{31}P) / ppm
001	-348.83	36.86	3.96	0.18	60.04
110	-343.25	38.36	13.19	0.64	156.10
100	-342.58	17.21	18.53	0.83	289.79
quartz-berlinite	-348.94	55.04	4.50	0.63	-30.16
buckled-berlinite	-348.96	38.99	8.99	0.39	-26.06